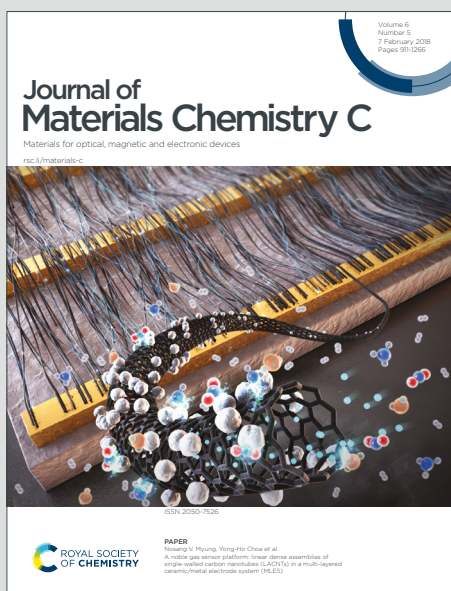


# Journal of Materials Chemistry C

Materials for optical, magnetic and electronic devices

Accepted Manuscript

This article can be cited before page numbers have been issued, to do this please use: T. Deng, Z. Ding, S. Zheng and R. Xie, *J. Mater. Chem. C*, 2025, DOI: 10.1039/D4TC05380J.



This is an Accepted Manuscript, which has been through the Royal Society of Chemistry peer review process and has been accepted for publication.

Accepted Manuscripts are published online shortly after acceptance, before technical editing, formatting and proof reading. Using this free service, authors can make their results available to the community, in citable form, before we publish the edited article. We will replace this Accepted Manuscript with the edited and formatted Advance Article as soon as it is available.

You can find more information about Accepted Manuscripts in the [Information for Authors](#).

Please note that technical editing may introduce minor changes to the text and/or graphics, which may alter content. The journal's standard [Terms & Conditions](#) and the [Ethical guidelines](#) still apply. In no event shall the Royal Society of Chemistry be held responsible for any errors or omissions in this Accepted Manuscript or any consequences arising from the use of any information it contains.

# Loss-Less $\text{La}_3\text{Si}_6\text{N}_{11}:\text{Ce}^{3+}$ Phosphor-in-Glass Color Converter by Using the Oxygen-Free Glass ZIF-62

View Article Online

DOI: 10.1039/D4TC05380J

## Converter by Using the Oxygen-Free Glass ZIF-62

Taoli Deng<sup>a,b</sup>, Zan Ding<sup>c</sup>, Shuang Zheng<sup>b</sup>, Rong-Jun Xie<sup>b\*</sup>

<sup>a</sup>College of Chemistry and Chemical Engineering, Anshun University, Anshun 561000, P. R. China

<sup>b</sup>Fujian Key Laboratory of Surface and Interface Engineering for High Performance Materials, College of Materials, Xiamen University, Xiamen 361005, P. R. China

<sup>c</sup>Guizhou University, Guiyang 550000, P. R. China

Email: [rjxie@xmu.edu.cn](mailto:rjxie@xmu.edu.cn)

**Abstract:**  $\text{Ce}^{3+}$ -doped nitride phosphors are promising color converters in laser-driven lighting and display technologies, but they confront from serious loss in luminescence efficiency caused by the interfacial reaction between phosphor powders and glass powders during the fabrication of phosphor-in-glass bulks or films. In this work, the oxygen-free organic-inorganic hybrid glass (OIHG)  $\text{Zn}(\text{Im})_3(\text{HbIm})$  (ZIF-62) was utilized instead of the traditional oxide glass to prepare the  $\text{La}_3\text{Si}_6\text{N}_{11}:\text{Ce}^{3+}$  (LSN) phosphor converter by cofiring LSN with the ZIF-62 glass. The LSN phosphor-in-ZIF-62 glass converter well maintains the internal quantum efficiency of the original phosphor powders, showing only a ~1% luminescence loss. The sandwich-structured LSN-in-ZIF-62 glass converter, constructed by cofiring it with sapphire substrates, enables to create a white lighting with a maximum luminous flux of 872.2 lm and luminous efficacy of 291 lm  $\text{W}^{-1}$  when pumped by a blue laser diode at a powder density of 5.99  $\text{W mm}^{-2}$ . The use of the oxygen-free ZIF-62 glass provides a viable method to design nitride phosphor-based color converters for low-power laser-driven lighting, high-power LED lighting or projection applications.

## 1. Introduction

Laser-driven solid-state lighting, by pumping phosphor converters with blue laser diodes, promises super-brightness and high-collimation white lighting sources, which have led to the development of next-generation lighting and display.<sup>1-9</sup> In this emerging technology, the phosphor converter is one of the key components to control the optical quality and service time of lighting sources, but it is still a big challenge to



design phosphor converters with excellent optical properties that can be survived from high-power density laser excitation. Among many types of phosphors, the nitride ones have received great attention due to their outstanding thermal stability and structural rigidity, thus making them to be promising converters in laser-driven lighting and display technologies.<sup>10-16</sup>

Currently, phosphor-in-glass (PiG) color converters are commonly used for laser lighting because they are easily prepared and have a low cost when compared to their counterparts such as single crystals and phosphor ceramics.<sup>17-20</sup> However, it is hard to prepare highly efficient nitride-PiG converters because nitride phosphor powders usually react with glass powders at firing temperatures, and their photoluminescence properties are then largely quenched (Table S1).<sup>12,21-24</sup> Therefore, to cofire nitride phosphors with glass powders into dense PiG color converters is an interesting topic but a difficult mission, which needs to be further investigated.

$\text{La}_3\text{Si}_6\text{N}_{11}:\text{Ce}^{3+}$  (LSN) is an excellent yellow-green phosphor with high quantum efficiency (QE) and thermal stability, and its emission can be redshifted by partial substitution of La with Y (*i.e.*, LYSN).<sup>25</sup> We prepared both LSN-PiG and LYSN-PiG films, and used them to produce high-brightness white and warm white laser lighting, respectively.<sup>12,26</sup> On the other hand, the loss in QE of LSN or LYSN is inevitably avoided because the nitride phosphor powders react with the melting oxide glass during cofiring. Although the oxidation reaction was effectively alleviated by uniformly coating the phosphor particles with hexagonal boron nitride (BN) to isolate the nitride phosphors from the glass matrix, internal quantum efficiency (IQE) of the LYSN-BN PiG films was still declined by 7.9% when compared to that of the original LYSN phosphor (*i.e.*, 77.9%  $\rightarrow$  70%). Therefore, it is necessary to find oxygen-free glass to totally prevent the reaction between phosphor and glass powders.

As we may know, the traditional glass can be mainly categorized into three types, *i.e.*, inorganic glasses, organic glasses and metallic glasses. They are dominated by mixed ionic-covalent bonds, covalent bonds and metallic bonds, respectively. The organic-inorganic hybrid glass (OIHG), considered as the fourth category of melt-quenched glasses, includes metal-organic framework crystals (MOFs), coordination polymers (CPs), metal-organic-inorganic complexes (MOCs) and metal coordination compounds (MCCs), which has recently demonstrated potential uses in gas separation, energy storage and optics application.<sup>27-35</sup> The OIHG presents a novel

View Article Online  
DOI: 10.1039/D4TC05380J



pathway for fabricating bulk functionalized structural materials, and its application in optics fields has been reported. For instance, Bennett *et al.* prepared the melt-quenched glass ZIF-62 of halide perovskites by the liquid-phase sintering, and found that the glass retained the exceptionally high efficiency of halide perovskite quantum dots and exhibited remarkable optical stability under various environmental conditions.<sup>36-38</sup> Qiu *et al.* successfully designed a variety of bulk optical materials based on MOCs combined with dyes and phosphors, which also demonstrate outstanding optical properties.<sup>28,31</sup>

In this work, to address the issue of oxidation-induced QE loss when nitride phosphors are cofired with traditional glasses, the OIHG, which can provide the oxygen-free sintering environment, is firstly synthesized and then cofired with nitride phosphor powders to form nitride-PiG films without luminescence loss as far as possible. The design of the nitride-PiG films by using the OIHG paves a way for applying nitride phosphor converters in low-power laser-driven lighting and displays, as well as high-power LED lighting.

## 2. Experimental Section

### 2.1 Fabrication of nitride-PiG bulks using the ZIF-62 OIHG

Materials: Phosphor of  $\text{La}_3\text{Si}_6\text{N}_{11}:\text{Ce}^{3+}$  (LSN:Ce, Mitsubishi Chemical Co., Ltd., Japan) was commercially available. The zinc nitrate hexahydrate ( $\text{Zn}(\text{NO}_3)_2 \cdot 6\text{H}_2\text{O}$ , Aladdin Reagent Co., Ltd., China), imidazole (Im, Aladdin Reagent Co., Ltd., China), benzimidazole (HbIm, Aladdin Reagent Co., Ltd., China), dimethylformamide (DMF, Aladdin Reagent Co., Ltd., China) and dichloromethane (DCM, Aladdin Reagent Co., Ltd., China) were all purchased. Single crystal sapphire plates with a size of  $14 \times 14 \times 1 \text{ mm}^3$  were bought from the Yuanfeng quartz products Co. Ltd. (China).

Firstly, the molar ratio of 3:25:5 of  $\text{Zn}(\text{NO}_3)_2 \cdot 6\text{H}_2\text{O}$ , Im and HbIm were added into 100 mL DMF. Then, the mixture was stirred at room temperature for 30 min, and subsequently transferred to a reaction autoclave for hydrothermal treatment. The treatment was done at  $130^\circ\text{C}$  for 60 h. Secondly, the reaction solution was centrifuged and filtered to obtain white crystalline powders, followed by washing with the DMF solution for three times and with DCM for two times. The washed white crystalline powders were activated in a tubular furnace under vacuum at  $150^\circ\text{C}$  for 72 h to complete the evaporation of residual DMF and DCM, and then the  $\text{Zn}(\text{Im})_3(\text{HbIm})$



(ZIF-62) powders were obtained.

View Article Online  
DOI: 10.1039/D4TC05380J

A certain molar mass ratio of ZIF-62 powders was thoroughly mixed with LSN:Ce phosphors. Specifically, the mass ratio of ZIF-62 to LSN:Ce was set at 2:1, 1:1, 3:2 and 1:2. Then the mixed powders were pressed into a circular bulk under a pressure of  $\sim 0.1$  MPa, with sapphire plates attached to both the top and bottom surfaces to construct a sandwich-structured phosphor converter. The sapphire plates were clamped with four stainless steel clips (*i.e.*, an approximate force of 200 N was applied). The assembled phosphor converter was placed in a tubular furnace, and heated to the desired temperatures (*i.e.*, 370, 380, 390 and 400°C) at a rate of 10°C/min in an Ar atmosphere. The holding time was 15 min. Then the sample was cooled naturally to room temperature to finally obtain the LSN-in-ZIF-62 glass converter. The detailed fabrication procedure of the sandwich-structured LSN-in-ZIF-62 converter is illustrated in Fig. 1a.

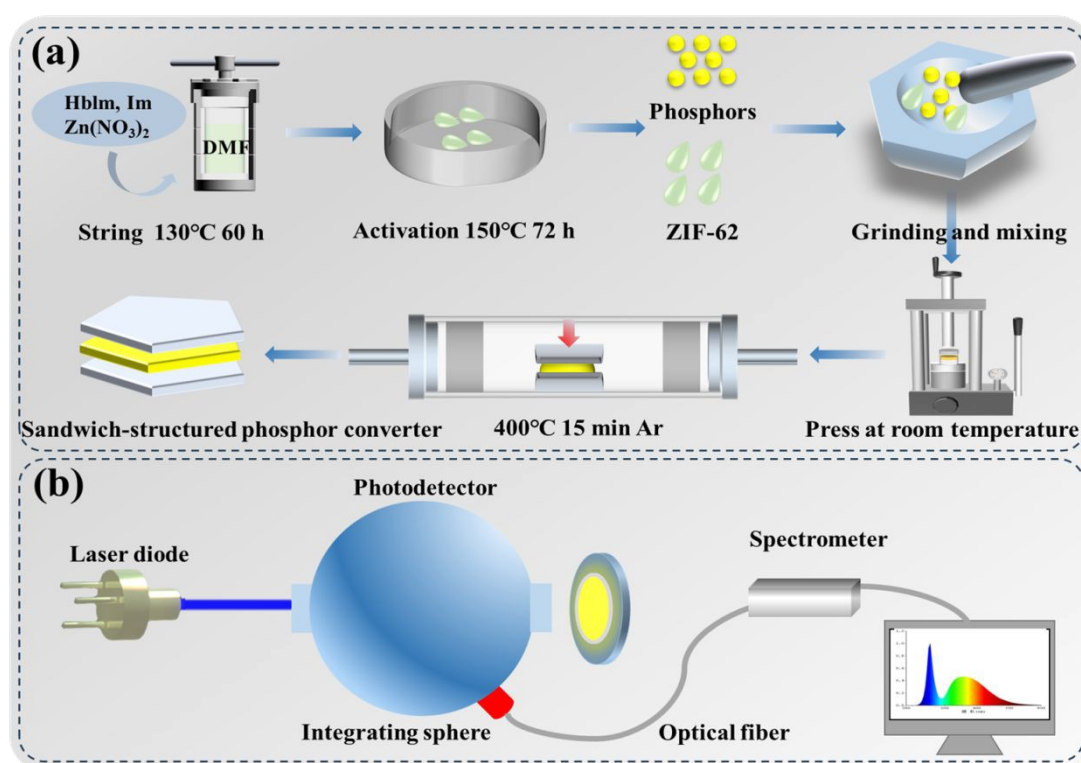


**Fig. 1** (a) Fabrication procedure of the sandwich-structured LSN-in-ZIF-62 glass converter. (b) Schematics of optical property measurement for the LSN-in-ZIF-62 glass converters under laser excitation.

## 2.2 Characterizations

The phase compositions of the ZIF-62 crystal, ZIF-62 glass and the



LSN-in-ZIF-62 glass converters were characterized by X-ray diffraction (D8 Advanced, Bruker, Germany) using Cu K $\alpha$  radiation at 40 kV, 40 mA. The microscopic morphology and elemental distribution mapping were obtained via Energy Dispersive Spectroscopy (EDS, X-MaxN, Oxford, UK) coupled with a Field Emission Scanning Electron Microscope (SEM, SU70, Hitachi, Japan). Fluorescence microscope images of LSN-in-ZIF-62 glass were recorded by a Fluorescence Microscope (DP74, OLYMPUS, Japan). The transmittance of the ZIF-62 glass was measured with an Ultraviolet-Visible Spectrophotometer (UV 3600 Plus, Shimadzu Corporation, Japan). The thermogravimetric analysis TG and DSC curves of the ZIF-62 crystal and glass were acquired from a Simultaneous Thermal Analyzer (STA, 449 F3 Jupiter, Netzsch, Germany). Infrared spectra of the ZIF-62 crystal and glass were measured by an infrared spectrometer (Nicolet is10, Thermo Fisher, USA).

Temperature-dependent emission spectra of the LSN-in-ZIF-62 glass converters were measured at temperatures ranging from 298 to 548 K using a system with a 450 nm LED light source, a charge-coupled device (CCD) spectrometer (USB2000+, Ocean Optics, USA), and a cooling-heating stage (THMS600E, Linkam, UK). The IQE of all samples were determined by a system consisting of an excitation light source (450 nm, 50 mW blue laser diode), an integrating sphere (diameter of 15 cm), and a CCD spectrometer (USB2000+, Ocean Optics, USA). Optical properties of the LSN-in-ZIF-62 glass converters under blue laser excitation were measured in a static reflective configuration by using a sphere-spectroradiometer system as shown in Fig. 1b, consists of a blue laser light source with an area of 0.5 mm<sup>2</sup> (LSR445CP-FC-48W, Lasever, China), an integrating sphere (diameter of 30 cm), and a CCD spectrometer (HR4000, Ocean Optics, USA).

### 3. Results and discussion

#### 3.1 Microstructure and properties of organic-inorganic hybrid glass ZIF-62

The ZIF-62 crystals were acquired through a hydrothermal method and further processed into an OIHG by a sintering process. The XRD pattern of ZIF-62 crystals presents sharp peaks, indicating a highly ordered crystalline structure as evidenced in Fig. 2a, and these peaks match well with the simulated diffraction pattern of the ZIF-62 crystals.<sup>39</sup> All characteristic diffraction peaks disappear after the ZIF-62



crystal being transformed into the ZIF-62 glass. The SEM image of the ZIF-62 crystal (Fig. 2b) shows it possess a block-like morphology with well-defined edges and a notably uniform particle distribution with the size of 10 ~ 20  $\mu\text{m}$ . Further, the EDS mapping corroborates that the elements Zn, N and C are uniformly dispersed throughout the ZIF-62 crystals as presented in Figs. 2c-f.

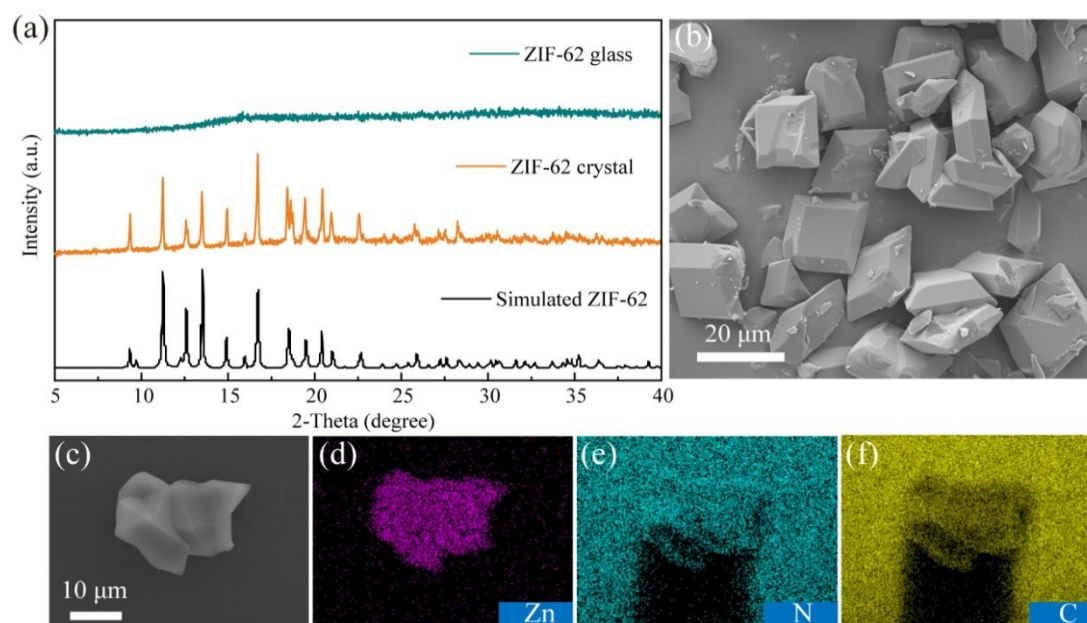


**Fig. 2** (a) XRD patterns of both the ZIF-62 crystal and glass. (b) SEM image of the ZIF-62 crystals. (c-f) Corresponding EDS mappings of Zn, N, and C elements.

The sintering process of the OIHG is crucial for preparing the PiG converter. Firstly, the tablet-shaped ZIF-62 crystals clamped with four stainless steel clips was sintered at 370, 380, 390 and 400 $^{\circ}\text{C}$  for 15 minutes in an Ar atmosphere. The actual photos of the sintered ZIF-62 glass are given in Fig. 3a. When the sintering temperature is 370 $^{\circ}\text{C}$ , only a small area in the middle appears transparency. The transmittance of the ZIF-62 glass is greatly enhanced and a large area turns transparency when the sintering temperature is further increased. After sintering at 400 $^{\circ}\text{C}$  for 15 min, the ZIF-62 glass shows a transmittance as high as ~87% in the visible light region (400-800 nm), which matches well with both the blue laser light and the converted light to improve the light extraction efficiency. The transmittance shows a dramatic drop below 400 nm (Fig. 3b).



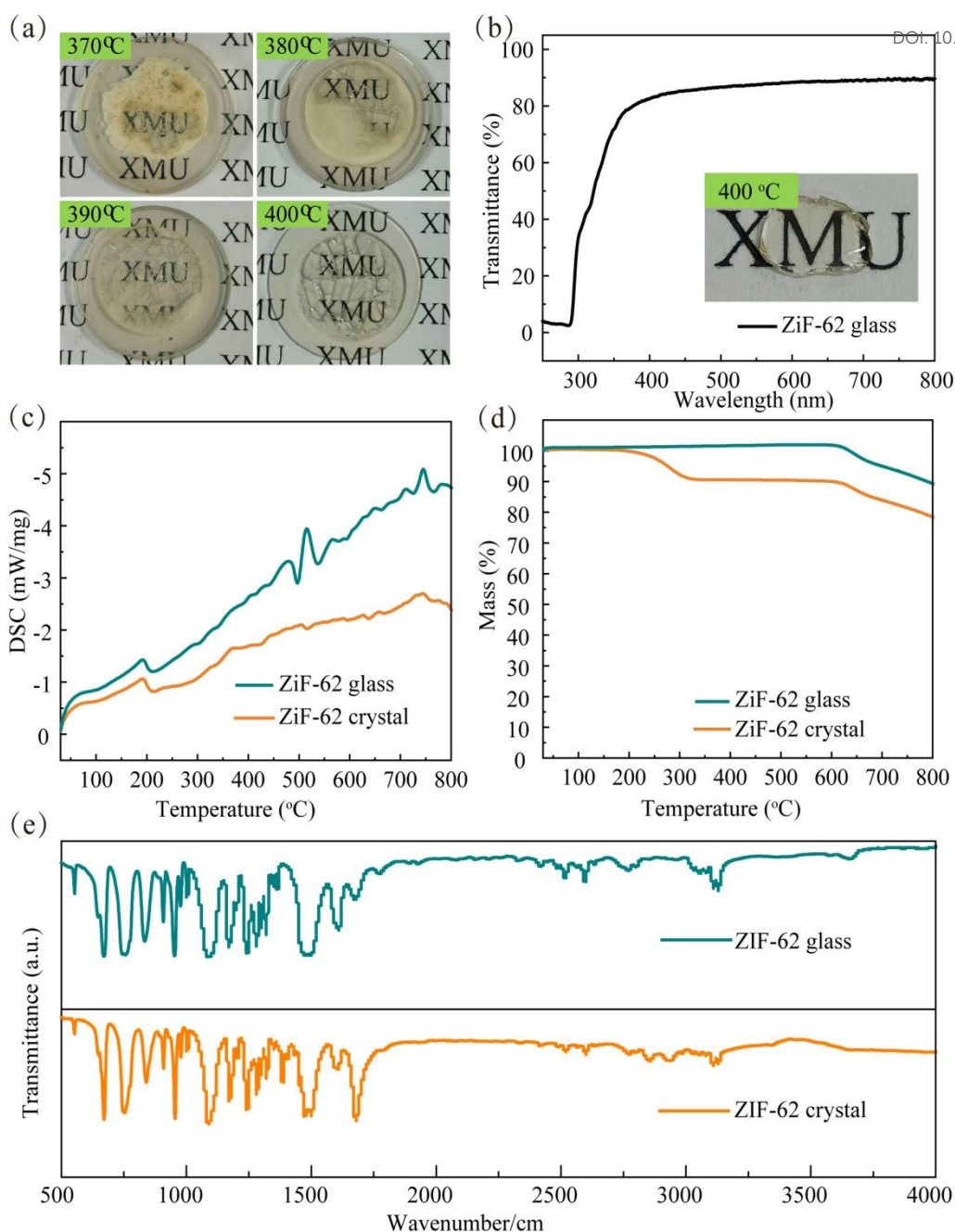


**Fig. 3** (a) Photos of the ZIF-62 glasses sintered at different temperatures. (b) Transmittance spectrum of the ZIF-62 glass sintered at 400°C. (c) DSC curves of the ZIF-62 crystal and ZIF-62 glass. (d) TG curves of the ZIF-62 crystal and ZIF-62 glass. (e) Infrared spectra of the ZIF-62 crystal and ZIF-62 glass.

The DSC and TG curves of the ZIF-62 crystals and ZIF-62 glass are presented in Figs. 3c-d, and it can be observed that the  $T_g$  of the ZIF-62 glass appears at 515°C, followed by the onset of the  $T_f$  at 715°C. In contrast, the DSC curve of the ZIF-62 crystals is relatively smooth, indicating the absence of phase transition or crystallization. Further, the TG curves of the ZIF-62 crystals and ZIF-62 glass reveal



that the thermal decomposition of the ZIF-62 crystals slowly occurs. Below 200°C there is virtually no mass loss, followed by a mass loss of approximately 12% between 200°C and 600°C. Subsequently, an additional mass loss occurs above 600°C, with the sample retaining 75% of its original mass at 800°C. On the other hand, the ZIF-62 glass exhibits remarkable thermal stability, with a negligible mass loss up to 580°C. Fig. 3e shows the infrared spectra of the ZIF-62 crystal and ZIF-62 glass. All functional group vibration characteristic peaks of both the ZIF-62 crystal and glass are at the same position, indicating that there is no chemical bond breakage or formation during the transformation of the ZIF-62 crystal into ZIF-62 glass.

### 3.2 Optical properties of the LSN-in-ZIF-62 glass converters

Thanks to the high transmittance and strong thermal stability of the ZIF-62 glass, a novel LSN-in-ZIF-62 glass converter was prepared. It can be seen from the photos that the glass converter has a flat surface and uniform color. Further, the fluorescence microscope image of the LSN-in-ZIF-62 glass converter shows that the LSN:Ce phosphor particles are evenly dispersed in the glass matrix as shown in Figs. 4a-b. A few pores are also seen in the glass matrix. The thickness of the LSN-in-ZIF-62 glass converter is ~80  $\mu\text{m}$  determined from the cross-section SEM image as shown in Fig. 4c. The SEM-EDS spectra demonstrate the distribution of the major elements La and Si from the phosphor particles, and Zn from the glass in the converter. A clear boundary between the LSN:Ce particle and the glass matrix is observed, indicating that no significant interfacial reaction occurs during the sintering process (Fig. 4d). In addition, the XRD pattern of LSN-in-ZIF-62 glass converter is presented in Fig. S1. After the transformation of ZIF-62 crystal into glass, all of the crystal characteristic diffraction peaks disappear, while the remaining major diffraction peaks can be matched well with the standard card of LSN phase (ICSD 248709).<sup>12</sup> It is worth noting that the LSN-in-ZIF-62 glass converter presents an outstanding thermal stability, which can maintain the photoluminescence intensity of over 90% at 250°C (Fig. 4e).



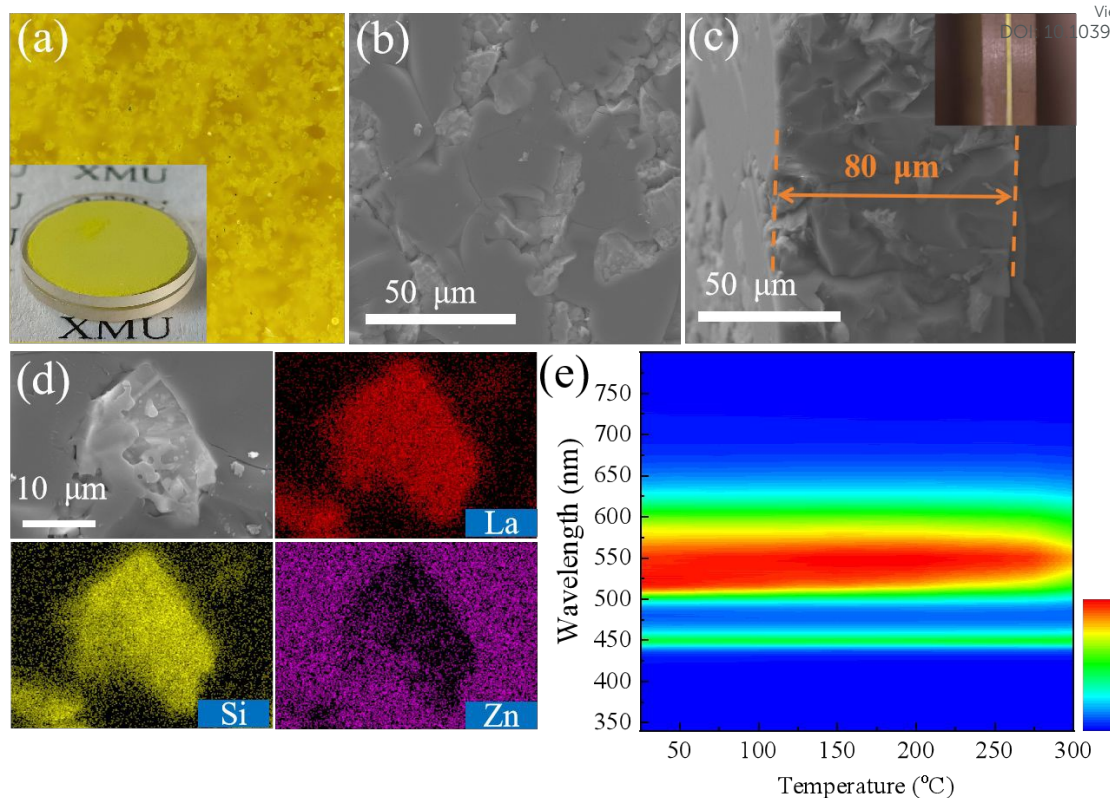


**Fig. 4** (a) Fluorescence microscope image (the photograph of the converter is the inset). (b) Top-view SEM image and (c) cross-section SEM image of the LSN-in-ZIF-62 glass converter (Photograph of the cross-sectional of the converter is the inset). (d) Corresponding EDS mappings of La, Si and Zn elements. (e) Temperature-dependent emission spectra of the glass converter.

The optical properties of the LSN-in-ZIF-62 glass converter with different mass ratios of the ZIF-62 glass to the LSN:Ce phosphor (i.e., 1:2, 1:1, 2:3 and 2:1) were evaluated. As shown in Fig. 5a where the IQE of the glass converters are presented, all the glass converters, having the highest IQE of 76.7%, exhibit a minimal IQE loss of  $\sim 1\%$  when compared to the original LSN:Ce powders. This strongly evidences that the LSN phosphor is protected by the oxygen-free ZIF-62 glass, and its IQE remains nearly unchanged after cofiring with the glass.



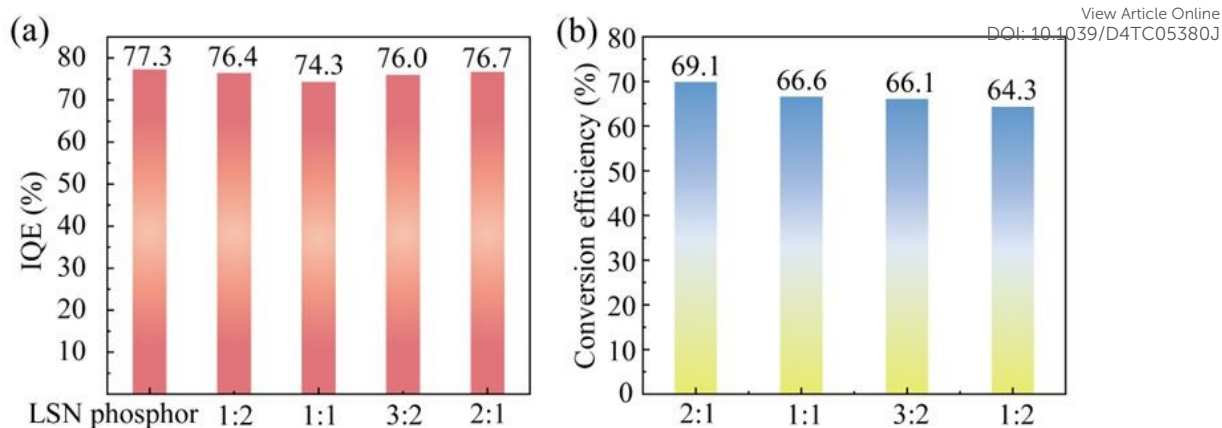


**Fig. 5** (a) IQE and (b) conversion efficiency of the LSN-in-ZIF-62 glass converter with different ratios of the glass to phosphor.

Owing to its high IQE and effective thermal management, the sandwich-structured LSN-in-ZIF-62 glass converter, with the ratio of the glass to the phosphor of 1:1, allows to prepare the laser-driven light source (CCT of 3860K, CRI of 60) with the maximum luminous flux of 872.2 lm and a luminous efficacy as high as 291.1 lm W<sup>-1</sup> under excitation with a laser power density of 5.99 W mm<sup>-2</sup> (Figs. 6a-b, Table S2). As seen in Figure 6c, the emission intensity of the LSN-in-ZIF-62 glass converter (ratio of the glass to phosphor is 1:1) monotonously increases as the incident laser power increases, and reach a maximum at 3 W. The light source illumination image of LSN-in-ZIF-62 glass converter under excitation of blue laser is shown in Fig. 6d. Moreover, the calculated conversion efficiency of the glass converters remains high and varies in the range of 64 - 69% (Fig. 5b). Finally, the aging test of the LSN-in-ZIF-62 glass converter was investigated under 85°C water vapor (Fig. 6e). The glass converter can still maintain a very high IQE more than 99% of its initial value even after aging for 612 hours, indicating that this novel glass converter possesses a long-term optical stability.



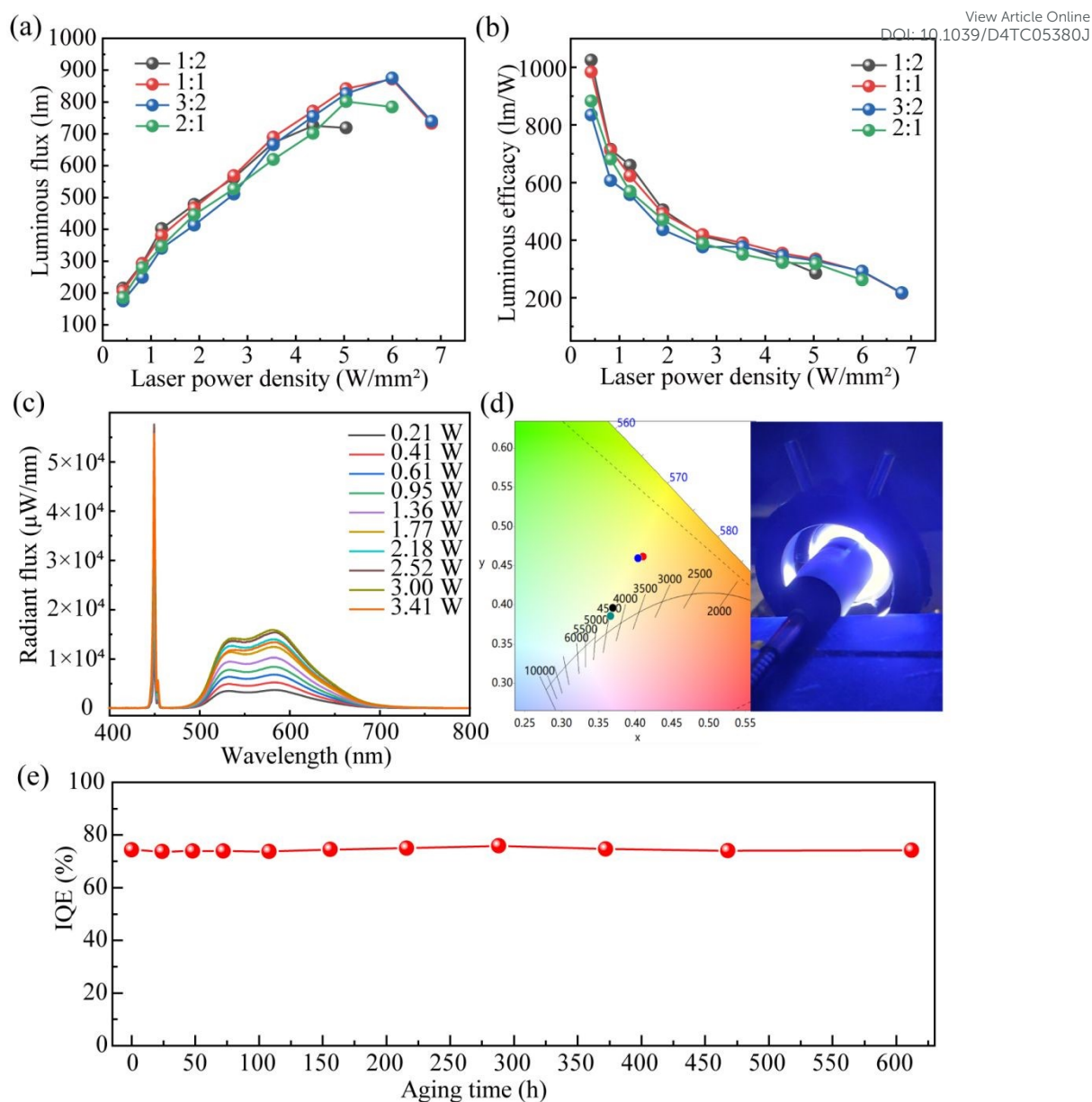


**Fig. 6** Optical performance of LSN-in-ZIF-62 glass converter with different ratios of the glass to phosphor (a-b) Luminous flux and luminous efficacy as a function with the laser power density. (c) Emission spectra of LSN-in-ZIF-62 glass converter (ratio of the glass to phosphor is 1:1). (d) the CIE color coordinates of LSN-in-ZIF-62 glass converter with different ratios of the glass to phosphor and illumination image of white light from the LSN-in-ZIF-62 glass converter under excitation of blue laser. (e) Aging test of the LSN-in-ZIF-62 glass converter.

The protection mechanism of the LSN phosphor by the ZIF-62 glass is illustrated in Fig. 7a. In addition, thanks to superior thermal conductivity and high transmittance of the sapphire substrate, the sandwich-structured LSN-in-ZIF-62 glass converter can mitigate the direct impact of high-density photons on the glass converter with effective thermal management under laser excitation (Fig. 7b).



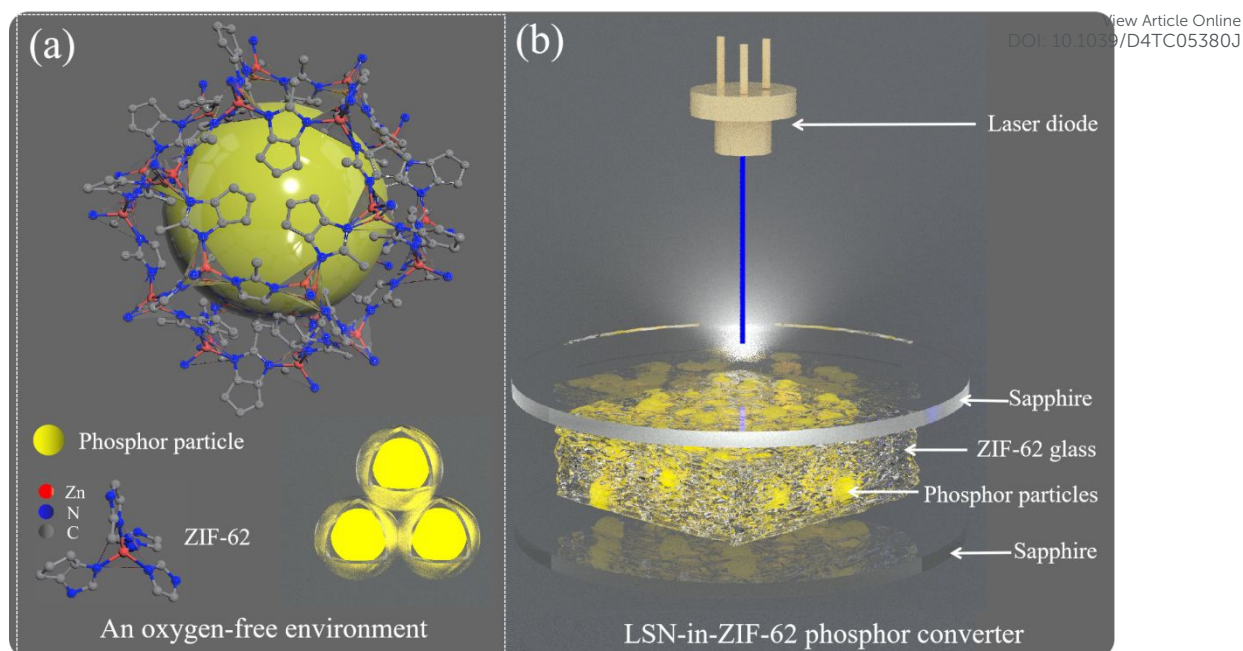


**Fig. 7** (a) The mechanism by the organic-inorganic glass ZIF-62 providing an oxygen-free sintering environment for protecting LSN:Ce phosphors. (b) Schematics of the laser-driven sandwich-structured LSN-in-ZIF-62 phosphor converter.

**Table 1** Optical properties of LSN-based color converters under laser irradiation

Samples	Luminous flux / lm	Luminous efficiency / lm·W <sup>-1</sup>	Saturation threshold / W·mm <sup>-2</sup>	Reference
LSN-PiG film	1076	166.05	12.9	12
LSN-PiG film	376.1	158	2.39 (W)	24
LSN-PiG	209	145.91	1.44	23
LSN-Al <sub>2</sub> O <sub>3</sub> -PiG film	3120	130	23.08	22
LSN	5602	102.04	21.96	40
PiGF@diamond	5602	102.04	21.96	40
LSN-in-ZIF-62 glass	872.2	291.1	5.99	This work

Table 1 summarizes the optical properties of some LSN-based PiG bulks or films under blue laser excitation. As seen, the LSN-in-ZIF-62 glass converter shows the highest luminous efficiency of 291.1 lm·W<sup>-1</sup> and a luminous flux of 872.2 lm even pumped by blue laser diodes with a small powder density of 5.99 W·mm<sup>-2</sup>. These interesting results are ascribed to the high IQE preserved by using the ZIF-62 glass and strong thermal management by using the sapphire substrate, enables relatively high luminous flux and luminous efficacy under low-power-density of LD excitation,



which is suitable for the low-power laser-driven lighting and displays, as well as high-power LED lighting applications. View Article Online  
DOI: 10.1039/D4TC05380J

#### 4. Conclusion

In this work, a LSN-in-ZIF-62 glass converter was designed and prepared by cofiring nitride phosphors with the OIHG at temperatures lower than 400°C. The oxygen-free sintering environment provided by the ZIF-62 glass enables to protect the nitride phosphor particles from oxidation, and the internal quantum efficiency and photoluminescence spectra of phosphors almost remain unchanged after cofiring with OIHG. The sandwich-structured LSN-in-ZIF-62 glass converter, constructed by using the sapphire substrates, showed enhanced thermal stability and allowed to create laser-driven white light with a luminous flux of 872.2 lm and a luminous efficacy of 291 lm·W<sup>-1</sup> when coupled to blue laser diodes with a power density of 5.99 W·mm<sup>-2</sup>. This work offers a viable method to design efficient nitride phosphor converters suitable for low-power laser-driven lighting as well as high-power LED lighting applications or projection applications.

#### Conflict of Interest

There is no conflict to declare.

#### CRedit authorship contribution statement

Taoli Deng: Data Curation, Formal analysis, Methodology, Investigation, and Writing-Original Draft. Zan Ding: Methodology, Formal analysis. Shuang Zheng: Investigation. Rong-Jun Xie: Conceptualization, Methodology, Writing-Review & Editing, Supervision, Funding acquisition.

#### Acknowledgment

This work is supported by the National Key Research and Development Program (MOST, 2022YFE0108800) and the Major Science and Technology Projects of Xiamen Science and Technology Bureau (No. 3502Z20231050).

#### Notes and references

- 1 S. X. Li, L. Wang, N. Hirotsaki, R.-J. Xie, *Laser Photonics Rev.* 2018, **12**, 1800173.
- 2 Y. G. Cao, R.-J. Xie, Q. L. Liu, X. Y. Chen, *Appl. Phys. Lett.* 2022, **121**, 150401.



- 3 P. Hu, Y. F. Liu, P. Sun, Z. H. Luo, J. Jiang, *Adv. Opt. Mater.* 2024, **12**, 2401672. [View Article Online](#)  
DOI: 10.1039/D4TC05380J
- 4 S. X. Liao, S. L. Jin, T. Pang, S. S. Lin, Y. H. Zheng, R. H. Chen, G. Y. Xi, X. Y. Li, B. Zhuang, F. Huang, D. Q. Chen, *Adv. Funct. Mater.* 2024, **34**, 2307761.
- 5 T. L. Deng, D. Halmurat, Z. T. Shen, T. Y. Yan, S. X. Li, L. Wang, R.-J. Xie, *Laser Photonics Rev.* 2023, **17**, 2300240.
- 6 C. C. Yang, X. Y. Zhang, J. Kang, C. Wei, P. F. Sang, S. H. Lin, B. H. Sun, J. T. Fan, B. X. Jiang, Y. Li, X. R. Chen, J. Xu, H. Chen, L. Zhang, *J Mater Sci Technol.* 2023, **166**, 1-20.
- 7 J. D. Zhang, H. S. Yang, Y. J. Zhang, X. D. Liu, Y. Q. Zhang, Y. Y. Liang, H. Li, B. Ma, X. J. Liang, W. D. Xiang, *Appl. Phys. Lett.* 2021, **119**, 023301.
- 8 G. Z. Li, Q. W. Pan, Z. H. Zhou, R. R. Gu, H. Zhang, X. J. Huang, G. P. Dong, X. D. Xiao, *Adv. Opt. Mater.* 2023, **11**, 2203028.
- 9 X. Y. Zhang, P. F. Sang, C. Wei, S. H. Lin, J. Kang, Y. B. Li, B. H. Sun, Y. Li, F. A. Selim, C. M. Zhou, T. Y. Zhou, S. W. Chen, C. F. Shi, W. Streck, H. Chen and L. Zhang, *J. Mater. Chem. C* 2024, **12**, 6046-6055.
- 10 S. X. Li, Q. Q. Zhu, L. Wang, D. M. Tang, Y. J. Cho, X. J. Liu, N. Hirosaki, T. Nishimura, T. Sekiguchi, Z. R. Huang, R.-J. Xie, *J. Mater. Chem. C* 2016, **4**, 8197-8205.
- 11 H. X. Chen, T. Lin, F. Huang, S. X. Li, X. Y. Tang, R.-J. Xie, *Adv. Opt. Mater.* 2022, **10**, 2200836.
- 12 S. H. You, S. X. Li, P. Zheng, T. L. Zhou, L. Wang, L. H. Liu, N. Hirosaki, F. F. Xu, R.-J. Xie, *Laser Photonics Rev.* 2019, **13**, 1800216.
- 13 S. H. You, S. X. Li, Y. C. Jia, R.-J. Xie, *Chem. Mater.* 2020, **32**, 3631-3640.
- 14 C. Y. Wang, T. Takeda, O. M. Ten Kate, R.-J. Xie, *J. Mater. Chem. C* 2016, **4**, 10358-10366.
- 15 L. Wang, R.-J. Xie, T. Suehiro, T. Takeda, N. Hirosaki, *Chem. Rev.* 2018, **118**, 1951-2009.
- 16 R. D. Tian, Q. H. Wang, S. X. Li, T. L. Zhou, R.-J. Xie, *J Mater Sci Technol.* 2025, **210**, 179-187.
- 17 S. X. Li, L. Wang, N. Hirosaki, R.-J. Xie, *Laser Photonics Rev.* 2018, **12**, 1800173.
- 18 Q. Q. Zhu, X. J. Wang, L. Wang, N. Hirosaki, T. Nishimura, Z. F. Tian, Q. Li, Y. Z. Xu, X. Xu, R.-J. Xie, *J. Mater. Chem. C* 2015, **3**, 10761-10766.
- 19 F. C. Xu, H. S. Yang, Y. J. Zhang, X. D. Liu, Y. Q. Zhang, L. S. Wang, Z. Wang,



- X. J. Liang, P. C. Qian, W. D. Xiang, *J Alloy Compd.* 2021, **887**, 161301. View Article Online  
DOI: 10.1039/D4TC05380J
- 20 S. X. Tao, Y. H. Ping, F. F. Huang, Y. J. Hua, P. Qiao, Y. G. Li, Z. C. Xu, H. P. Ma, *Ceram. Int.* 2023, **49**, 19606-19614.
- 21 T. Lin, H. X. Chen, S. X. Li, L. Wang, F. Huang, R.-J. Xie, *Chem. Eng. J.* 2022, **444**, 136591.
- 22 M. H. Huang, Q. Q. Zhu, S. X. Li, Y. Zhai, H. Zhang, L. Wang, R.-J. Xie, *J. Mater. Chem. C* 2023, **11**, 488-496.
- 23 L. Xu, L. H. Wang, S. Y. Bao, Y. Wang, J. D. Zhang, Y. Y. Liang, X. J. Liang, Q. Chen, W. D. Xiang, *Ceram. Int.* 2022, **48**, 23955-23962.
- 24 Z. K. Yu, J. Z. Zhao, J. X. Liu, Y. Mou, M. X. Chen, Y. Peng, *Ceram. Int.* 2022, **48**, 36531-36538.
- 25 F. Du, W. D. Zhuang, R. H. Liu, Y. H. Liu, J. Y. Zhong, W. Gao, K. Chen, L. Chen, K. Kato, K. Lin, *RSC Adv.* 2016, **6**, 77059-77065.
- 26 T. L. Deng, L. H. Huang, S. X. Li, Q. Q. Zhu, L. Wang, T. Takeda, H. Naoto, R.-J. Xie, *Laser Photonics Rev.* 2022, **16**, 2100722.
- 27 A. Qiao, T. D. Bennett, H. Z. Tao, A. Krajnc, G. Mali, C. M. Doherty, A. W. Thornton, J. C. Mauro, G. N. Greaves, Y. Z. Yue, *Sci. Adv.* 2018, **4**, eaao6827.
- 28 M. A. Ali, X. F. Liu, B. B. Xu, Y. Li, M. A. Mohamed, Y. Z. Yue, J. R. Qiu, *ACS Materials Lett.* 2022, **4**, 2613-2621.
- 29 M. A. Ali, W. M. Winters, M. A. Mohamed, D. Z. Tan, G. J. Zheng, R. S. Madsen, O. V. Magdysyuk, M. Diaz-Lopez, B. Cai, N. Gong, Y. J. Xu, I. V. Hung, Z. H. Gan, S. Sen, H. T. Sun, T. D. Bennett, X. F. Liu, Y. Z. Yue, J. R. Qiu, *Angew. Chem. Int. Edit.* 2023, **62**, e202218094.
- 30 J. J. Yan, C. W. Gao, S. B. Qi, Z. J. Jiang, L. R. Jensen, H. B. Zhan, Y. F. Zhang, Y. Z. Yue, *Nano Energy* 2022, **103**, 107779.
- 31 M. A. Ali, X. F. Liu, H. T. Sun, J. J. Ren, J. R. Qiu, *Chem. Mater.* 2022, **34**, 2476-2483.
- 32 H. Z. Tao, T. D. Bennett, Y. Z. Yue, *Adv. Mater.* 2017, **29**, 1601705.
- 33 Y. J. Zhao, L. Y. Zhu, Y. Q. Kang, C.-H. Shen, X. Y. Liu, D. Jiang, L. Fu, O. Gusel'nikova, L. J. Huang, X. K. Song, T. Asahi, Y. Yamauchi, *ACS Nano* 2024, **18**, 22404-22414.
- 34 X. D. Liu, E. R. Mei, Z. Z. Liu, J. Du, X. J. Liang, W. D. Xiang, *ACS Photonics* 2021, **8**, 887-893.
- 35 J. Huang, J. J. Zhou, E. Jungstedt, A. Samanta, J. Linnros, L. A. Berglund, I.



Sychugov, *ACS Photonics* 2022, **9**, 2499-2509.

View Article Online  
DOI: 10.1039/D4TC05380J

- 36 R. J. Lin, M. L. Chai, Y. H. Zhou, V. C. Chen, T. D. Bennett, J. W. Hou, *Chem. Soc. Rev.* 2023, **52**, 4149-4172.
- 37 J. W. Hou, P. Chen, A. Shukla, A. Krajnc, T. S. Wang, X. M. Li, R. Doasa, L. H. G. Tizei, B. Chan, D. N. Johnstone, R. J. Lin, T. U. Schüllli, I. Martens, D. Appadoo, M. S. Ari, Z. L. Wang, T. Wei, S. C. Lo, M. Y. Lu, S. C. Li, E. B. Namdas, G. Mali, A. K. Cheetham, S. M. Collins, V. Chen, L. Z. Wang, T. D. Bennett, *Science* 2021, **374**, 621-625.
- 38 O. Smirnova, R. Sajzew, S. J. Finkelmeyer, T. Asadov, S. Chattopadhyay, T. Wieduwilt, A. Reupert, M. Presselt, A. Knebel, L. Wondraczek, *Nat. Commun.* 2024, **15**, 5079.
- 39 S. Li, R. Limbach, L. Longley, A. A. Shirzadi, J. C. Walmsley, D. N. Johnstone, P. A. Midgley, L. Wondraczek, T. D. Bennett, *J. Am. Chem. Soc.* 2019, **141**, 1027-1034.
- 40 Z. K. Yu, J. Z. Zhao, Z. Z. Yang, Y. Mou, H. J. Zhang, R. P. Xu, Q. Wang, L. W. Zeng, L. Lei, S. S. Lin, H. Li, Y. Peng, D. Q. Chen, M. X. Chen, *Adv. Mater.* 2024, **36**, 2406147.



## Data availability statements

The data supporting this article have been included as part of the Supplementary Information.

